Acetamide-Caprolactam Deep Eutectic Solvent-Based Electrolyte for Stable Zn-Metal Batteries

Shihe Wang, Ganxiong Liu, Wang Wan, Xueyang Li, Ju Li,* and Chao Wang*

Aqueous Zn-ion batteries (AZIBs) are promising for grid-scale energy storage. However, conventional AZIBs face challenges including hydrogen evolution reaction (HER), leading to high local pH, and by-product formation on the anode. Hereby the hydrogen bonds in the aqueous electrolyte are reconstructed by using a deep eutectic co-solvent (DES) made of acetamide (H-bond donor) and caprolactam (H-bond acceptor), which effectively suppresses the reactivity of water and broadens the electrochemical voltage stability window. The coordination between Zn^{2+} and acetamide-caprolactam in DES-based electrolytes produces a unique solvation structure that promotes the preferential growth of Zn crystals along the (002) plane. This will inhibit the formation of Zn dendrites and ensure the uniform deposition of Zn-ions on the anode surface. In addition, it is found that this DES-based electrolyte can form a protective membrane on the anode surface, reducing the risks of Zn corrosion. Compared to conventional electrolytes, the DES-based electrolyte shows a long-term stable plating/stripping performance with a significantly improved Coulombic efficiency from 78.18% to 98.37%. It is further demonstrated that a Zn||VS$_2$ full-cell with the DES-based electrolyte exhibits enhanced stability after 500 cycles with 85.4% capacity retention at 0.5 A g^{-1}.

1. Introduction

With the ever-increasing demand for reliable grid-scale energy storage, aqueous Zn-ion batteries (ZIBs) arouse great attention for their low cost, environmental friendliness, and innate safety.[1] Zn metal is a promising anode for ZIBs due to

S. Wang, G. Liu, W. Wan, X. Li, C. Wang
School of Materials Science and Engineering
Tongji University
Shanghai 201804, China
E-mail: chaow@tongji.edu.cn
J. Li
Department of Materials Science and Engineering and Department of Nuclear Science and Engineering
Massachusetts Institute of Technology
Cambridge, MA 02139, USA
E-mail: liju@mit.edu

The ORCID identification number(s) for the author(s) of this article can be found under https://doi.org/10.1002/adma.202306546

its high gravimetric and volumetric capacities (820 mAh g^{-1} and 5855 mAh cm^{-3}, respectively), low electrochemical potential (−0.762 vs SHE), and earth abundance.[2] Zn is an amphoteric metal that cannot withstand either acidic or alkaline environments. In aqueous electrolytes, the reduction potential of Zn^{2+} to Zn is quite adjacent to the potential for the hydrogen evolution reaction (HER). As a result, HER was inevitable during Zn deposition, which can increase the local pH, cause corrosion of the Zn anode, and result in the formation of by-products, such as $Zn(OH)_2$, $Zn_4(OH)_6SO_4 \cdot nH_2O$, and $Zn_x(OTf)_y(OH)_{2x+y} \cdot nH_2O$.[3] Additionally, the strong binding energy between solvated Zn-ions and (101) crystal plane causes a preference for vertical deposition.[4] These results in the formation of Zn dendrites, which can lead to short-circuiting of the battery, posing significant safety risks. The large surface area of dendritic Zn can decrease the Coulombic efficiency (CE), resulting in rapid capacity fading, which makes it challenging to fully utilize the capacity of the Zn anode (low depth of discharge, DOD).[5]

Several strategies have been proposed to address issues of Zn stability, gas evolution, and dendrite growth for achieving high-performance Zn-ion batteries.[6] Among these strategies, electrolyte modification has proven to be the most efficient and practical method for achieving uniform Zn deposition and reducing side reactions.[7] In aqueous electrolytes, water molecules form a highly dynamic and disordered solvation structure around the ions. This dynamic solvation structure makes it easier for water molecules to undergo oxidation or reduction reactions, which can lead to the breakdown of the electrolyte and the formation of unwanted by-products.[8]

The original objective of electrolyte design was to optimize the deposition mode of Zn-ion by compressing the electric double layer to decrease the electrostatic repulsion of Zn^{2+}, which proved to be effective in stabilizing the anode.[9] However, with the help of molecular dynamics (MD) simulations, researchers were able to gain a deeper understanding of the solvation structure of Zn-ion.[10] This newfound understanding has empowered them to effectively regulate the diffusion and deposition processes of Zn^{2+}, while concurrently mitigating the reactivity of water.[11] Therefore, significant progress has been made in

**ADVANCED
SCIENCE NEWS**

www.advancedsciencenews.com

**ADVANCED
MATERIALS**

www.advmat.de

modulating the solvation structure, such as using high-concentration solutions to attract free water molecules tightly,[12] investigating the use of acetonitrile as a solvent,[13] and developing deep eutectic solvents with a favorable coordination structure with Zn^{2+}, etc.[14] For instance, Suo et al. achieved a breakthrough in the electrochemical window limit of aqueous electrolytes (1.23 V) by using extremely high-concentration solutions of salt in water. A large number of solvated ions tightly attracted free water in the electrolyte, thus inhibiting the evolution of hydrogen and oxidation of the electrolyte.[12] Reza et al. investigated acetonitrile as an efficient solvent for reversible Zn plating/stripping. They found that using an anhydrous coordination structure in acetonitrile can prevent corrosion and enhance the stability of the electrode-solution surface, resulting in high Coulombic efficiency and low polarization.[13]

Deep eutectic solvents (DES) are unique types of solvents that are formed by mixing two or more components that interact through hydrogen bonding.[15] This results in a solvation structure that is different from traditional solvents such as water or organic solvents. DES-based electrolytes have been found to possess a broader stable window compared to aqueous electrolytes, largely due to their stable and ordered solvation structure.[16] This structure is conducive for coordinating with Zn^{2+} ions, thereby enabling the reshaping of the compact inner solvation layer with fewer active H_2O molecules. As a result, Zn deposition on the electrode surface becomes more uniform, which improves the efficiency and consistency of the electroplating process. Moreover, the solvation structure of DES mitigates undesirable reactions, thereby extending the stability and electrochemical window of the electrolyte. For example, Zhou et al. applied methylsulfonylmethane as the organic ligand to form an optimized hydrated eutectic electrolyte. This design can effectively restrain the reactivity of water, promoting smooth Zn-ions deposition.[17] Conversely, Ciucci et al. developed a novel deep eutectic electrolyte comprising sulfolane and $Zn(ClO_4)_2 \cdot 6H_2O$. Owing to the robust restriction of active water by DES, this electrolyte can withstand a broad operating temperature and voltage range.[18] Although DESs are economically viable, non-flammable, and stable, they are characterized by high binding energy, which gives rise to considerable viscosity. This, in turn, can induce significant polarization and decelerate dynamics.[19] To address this issue, researchers are exploring the use of small molecule cosolvents with strong polarity, low viscosity, and a large dielectric constant.[20] Water molecules is an obvious choice. However, in order to achieve the optimal solvation structure and ionic conductivity, the water content within the electrolyte needs to be rigorously controlled.

To ensure the stability and reversibility of the Zn anode, an ideal electrolyte should possess four key characteristics. Firstly, it should be chemically stable and refrain from corroding the reactive Zn, which can be vulnerable in both acidic and basic conditions. Secondly, water reactivity in the electrolyte should be curtailed to prevent unwanted HER, which could pose safety risks and diminish energy efficiency. Thirdly, the solvation structure of the electrolyte should facilitate the even deposition of Zn^{2+} and slow down the deterioration rate of the Zn anode. Lastly, the electrolyte should exhibit good ion conductivity and excellent wettability to prevent significant polarization.

In this study, we develop a novel DES-based aqueous electrolyte consisting of 50% acetamide (C_2H_5NO)-caprolactam ($C_6H_{11}NO$) with a molar ratio of 1:1 and 50 vol% water as the co-solvent, in addition to 1 molar $Zn(OTf)_2$ as the solute (DES50 electrolyte). For comparison, the control electrolyte contains only water as the solvent. Acetamide and caprolactam demonstrate robust coordination with Zn^{2+} ions, which consequently reduces the water content in the Zn^{2+} solvation structure and minimizes the reactivity of free water, thus suppressing HER. Furthermore, the DES is capable of polymerizing in situ on the Zn anode surface, thereby forming a Zn-ion conductive protective layer. This layer mitigates side reactions between amphoteric Zn and the electrolyte and controls the distribution of Zn^{2+} ions on the Zn foil surface. The in situ formed surface layer, together with the DES-based electrolyte, assists in regulating the uniform deposition of the Zn crystal plane, particularly inducing the growth of the Zn (002) plane.

DES-based electrolytes exhibit lower vapor pressure and deliver more stable and consistent performance. Compared to the control group electrolyte, the DES50 electrolyte displays a lower HER onset potential of over 200 mV and a higher Coulombic efficiency of 98.37% in the Zn||Ti cell. The electrolyte achieves a lifespan of 2000 h at a current density of 1 mA cm^{-2} and an area capacity of 1 mAh cm^{-2} in a Zn||Zn symmetric cell. It also has a lifespan of 1000 h at a current density of 10 mA cm^{-2} and an area capacity of 10 mAh cm^{-2}. When paired with a vanadium disulfide (VS$_2$) cathode to form a full cell, it delivers a capacity retention of 85.4% after 500 cycles in 0.5 A g^{-1} and 89.9% after 150 cycles in 0.1 A g^{-1}.

2. Results and Discussion

2.1. Physical and Chemical Properties of DES-Based Electrolytes

As shown in **Figure 1**a, the deep eutectic solvent (DES) was prepared by mixing caprolactam and acetamide in a 1:1 molar ratio and heating the mixture at 60 °C until it liquefied. The DES was then cooled to room temperature while maintaining its liquid state. It is worth noting that the molar ratio of these two substances will significantly influences the hydrogen bond network within the liquid, as demonstrated by the temperature difference in the eutectic point. We characterized this difference using Differential Scanning Calorimetry (DSC), and the results indicate that when the molar ratio of the two is 1:1, the eutectic temperature is the lowest. In other words, at this ratio, the ability to modify the solvation structure is the strongest (Figure S1, Supporting Information). To demonstrate DES's ability to dissolve Zn salt and control the coordination structure of solvated Zn-ion, Fourier Transform Infrared (FTIR) spectroscopy was used to identify the distinctive functional groups in the solutions. As shown in Figure 1b and Figure S2 (Supporting Information), the DES solvent was infused with $Zn(OTf)_2$ at various concentrations ranging from 0 to 1.25 mol L^{-1}. We observed that several of the characteristic absorption peaks of $Zn(OTf)_2$ lessen in the solutions, indicating the successful solvation of Zn salt. As the Zn salt concentration increased, the C = O stretching vibration from DES shifted from 1656 to 1637 cm^{-1}, suggesting a high carbonyl oxygen solvation degree. This further confirms the strong affinity between Zn-ion and DES.[19] Nonetheless, the DES-based electrolyte demonstrated increased viscosity following the dissolution of the Zn salt. Thus, the concentration of Zn salt is set

2306546 (2 of 10)
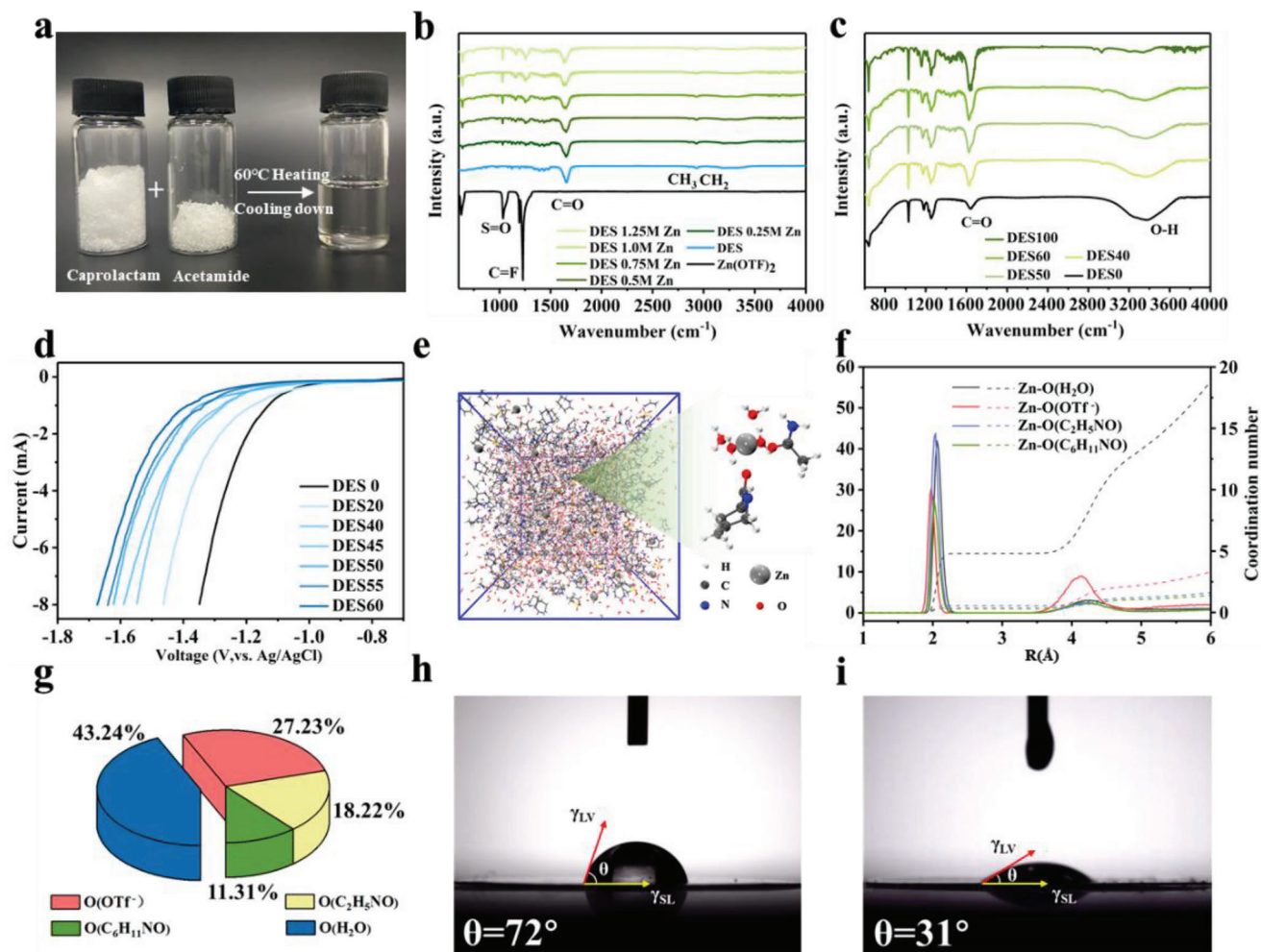
Figure 1. Eutectic electrolyte structure analysis a) Formation process of deep eutectic solvent; FT-IR spectra of DES b) with gradient concentration of Zn(OTf)$_2$; c) with 1 M Zn(OTF)$_2$ adding gradient volume fraction of H$_2$O; d) LSV curve of Zn anode in different DES electrolytes at a scan rate of 1 mV s^{-1}; e) 3D snapshot obtained by MD simulations and representative Zn^{2+}-solvation structure of DES50; f) RDFs for Zn–O(H$_2$O), Zn–O(OTf$^-$), Zn–O(C$_2$H$_5$NO), Zn–O(C$_6$H$_{11}$NO) with a coordination number of Zn^{2+} from MD simulations and g) distribution of coordination in primary solvation sheath in DES50. The contact angle of h) DES0 and i) DES50 in Zn foils.

to 1 mol L^{-1}. As illustrated in Figure 1c, the C = O absorption peak becomes more prominent as the DES ratio in the electrolyte increases. This observation confirms the disruption of the water-isolated structure. Additionally, the intensification of O–H stretching vibration, shifting toward higher wavenumbers, signifies an enhancement in the bonding ability of O–H groups. This strengthening of O—H bonds contributes to the reduction in free water activity. Linear sweep voltammetry (LSV) was conducted to evaluate the HER behavior of the DES-based electrolytes with varying DES contents (DES20, DES40, DES45, DES50, DES55, and DES60) compared with the control group (1 M Zn(OTf)$_2$ in H$_2$O, referred to as DES0). As illustrated in Figure 1d, the onset potential of HER decreased as the proportion of DES in the solution increases. Notably, the DES50 electrolyte displays a delayed HER potential of over 270 mV at a current of 8 mA cm^{-2} compared to the DES0 electrolyte.

To determine the optimal ratio of DES in electrolytes for ensuring the reversibility of the Zn anode, we conducted electrochem-

ical tests on a range of electrolytes (DES35 to DES60) in Zn symmetric cells operating under 10 mA cm^{-2} and 10 mAh cm^{-2} conditions (Figure S3, Supporting Information). The results clearly demonstrated that DES50 electrolytes exhibited an exceptional cycle life, surpassing 600 h. Therefore, DES50 was determined to be the optimal electrolyte in our study. This selection is the result of a delicate balance between various factors, including solvation strength, ionic conductivity, viscosity, and more. When the proportion of DES is too low, the solvation effect is insufficient, which compromises the protection of the zinc metal. Conversely, if the proportion of DES is too high, challenges such as increased viscosity and decreased conductivity (as shown in Figure S4, Supporting Information) can arise, adversely affecting battery cycling performance.

Molecular dynamics (MD) simulations can provide insights into the solvation structures of Zn^{2+} in DES50 systems, revealing the reduced presence of water molecules. In DES50 systems, the amides successfully enter the Zn^{2+} solvation

**ADVANCED
SCIENCE NEWS**

www.advancedsciencenews.com

**ADVANCED
MATERIALS**

www.advmat.de

structure, resulting in reduced water content in the solvation structure (Figure 1e). The corresponding radial distribution functions (RDFs) and coordination analysis presented in Figure 1f demonstrate distinct peaks at ≈2 Å, indicating the presence of $Zn-O(H_2O)$, $Zn-O(OTf^-)$, $Zn–O(C_2H_5NO)$, $Zn–O(C_6H_{11}NO)$ in the first solvation shell of Zn^{2+}, and the average coordination number for these solvation species are 2.59, 1.63, 1.09, and 0.68 respectively. Conversely, in DES0 systems, Zn^{2+} remains well hydrated, forming a network of water clusters through strong hydrogen bonds (Figure S5, Supporting Information) and the solvation structure is dominated by $Zn–O(H_2O)$ coordination (Figure S6a, Supporting Information). The coordination proportion of water is significantly reduced from 61.5% in DES0 to 43.2% in DES50 (Figure 1g and Figure S6b, Supporting Information), effectively impeding the migration of solvated water molecules with Zn ions and suppressing the occurrence of HER during the Zn deposition process.

The DES50 electrolyte exhibits improved wettability on Zn foil in comparison to DES0, as evidenced by the smaller contact angle observed in DES50 (31°) compared to DES0 (72°) (Figure 1h,i). This enhanced wettability has the potential to facilitate interfacial mass transfer processes, leading to significantly lower interfacial resistance for DES50 compared to DES0 after a 2-h rest period (Figure S7, Supporting Information). Additionally, the DES50 electrolyte demonstrates enhanced thermal stability. It shows that the glass fiber separator catches fire and deforms severely when lit with a lighter, while it remains unaffected when saturated with DES50, maintaining its integrity throughout the fire test (Figure S8 and Movie S1, Supporting Information).[21] This indicates that the inclusion of DES maintains the inherent safety performance of the electrolyte. What is more, the DES based on caprolactam and acetamide offers significant cost advantages compared to other eutectic solvents, as demonstrated in Figure S9 and Table S1 (Supporting Information).

The caprolactam and acetamide-based deep eutectic solvent (DES) electrolytes exhibited a reduced presence of water molecules in the solvation structure of Zn^{2+}, effectively preventing undesired reactions during the Zn deposition process. Among the different DES compositions studied, DES50 emerged as the optimal electrolyte due to its significantly delayed onset potential of the hydrogen evolution reaction (HER), improved wettability on Zn foil, and enhanced thermal stability. These properties make DES50 a safer and more favorable choice for electrolyte applications.

2.2. Zn Stability in DES-Based Electrolyte

DES50 demonstrates better stability with Zn metal foils than DES0 electrolyte. Cyclic voltammetry (CV) measurements at different sweep speeds were used to investigate the variation of double-layer capacitance of the fresh cells (Figure S10, Supporting Information). The results reveal that the DES50 group exhibits an ≈50% reduction in capacitance compared to the DES0 group. This reduction indicates a decrease in charge consumption during the non-Faradaic process, resulting in reduced voltage lag and lower excessive internal energy consumption during cycling. Moreover, after immersing the Zn metal foil in both DES0 and DES50 electrolytes for 30 days at 60 °C, noticeable dif-

ferences in the surface condition are observed (**Figure 2**a). The Zn foil immersed in DES0 develops a thick and loose corrosion layer, resulting in the formation of small bumps. In contrast, the foil immersed in DES50 shows a thinner corrosion layer and remains macroscopically smooth. The SEM cross-section images provide further evidence to support our findings (Figure 2b,c). After immersion in the DES0 electrolyte, the surface of the Zn foil exhibited excessive corrosion products and a loose film. In contrast, the DES50 electrolyte resulted in the formation of a dense and uniform protective layer on the Zn foil's surface. Additionally, it's worth noting that the thickness of the surface film is ≈1 μm after a 24-h immersion (Figure S11, Supporting Information). Moreover, X-ray diffraction (XRD) analysis (Figure S12, Supporting Information) demonstrates strong characteristic peaks associated with $Zn_x(OTf)_y(OH)_{2x+y}·nH_2O$ by-products are present in the DES0 group, whereas the Zn foil in the DES50 group maintains a pristine surface, highlighting its enhanced stability.

The non-faradaic capacitance obtained from the CV curve provides a quantitative analysis of the surface area.[22] Upon examining the CV results in Figure 2d,e, it is evident that the interface capacitance of the Zn||Zn symmetric cells increases after resting for 0, 14, and 30 days, indicating an expansion of the surface area due to electrolyte corrosion. Detailed calculations of the specific capacitance can be found in the Supporting Information. The accumulation of corrosion by-products over time results in an enlargement of the ineffective interfacial surface area. Importantly, it is notable that the DES50 group exhibits a more stable variation in the interfacial capacitance, while the increase in capacitance is more prominent in the DES0 group compared to the DES50 group, indicating a more severe side-reaction in DES0, which aligns with our previous analysis. Furthermore, the cell with DES50 as the electrolyte exhibits lower impedance variation during immersion compared to the DES0 group (Figure S13, Supporting Information), indicating a more stable and efficient electrochemical interface. This further underscores its superior performance compared to DES0.

To more accurately assess the impact of electrolytes on the kinetics of Zn anode corrosion, a Tafel test was performed using a three-electrode system (Figure S14, Supporting Information). Fitting the linear polarization region data reveals that the DES50 exhibits a self-corrosion potential closer to a positive value and a significantly lower corrosion current density compared to DES0. These findings indicate that DES50 has a lower tendency and slower rate of corrosion. This enhanced anti-corrosion ability can be attributed to the formation of a protective solid electrolyte interphase (SEI) membrane on the surface of the Zn electrode.

The film formation process can be described in three distinct steps, as depicted in Figure 2f. Initially, instead of directly losing electrons to become Zn-ions, the Zn metal undergoes interaction with the carbonyl oxygen atom, facilitating the transfer of its charge to the amino-N and resulting in a positive charge. Subsequently, the amino-N of the active species, with an excess of electrons, acts as a nucleophile, attacking the carbonyl oxygen atom of the caprolactam monomer. Finally, acetamide acts as a sealing agent, binding to the polymer chain through its amino and carbonyl functional groups, effectively halting the polymerization process and releasing Zn atoms. The overall polymerization process can be described by Equation (1), where n moles of caprolactam and 1 mole of acetamide polymerize to form

**ADVANCED
SCIENCE NEWS**
www.advancedsciencenews.com

**ADVANCED
MATERIALS**
www.advmat.de
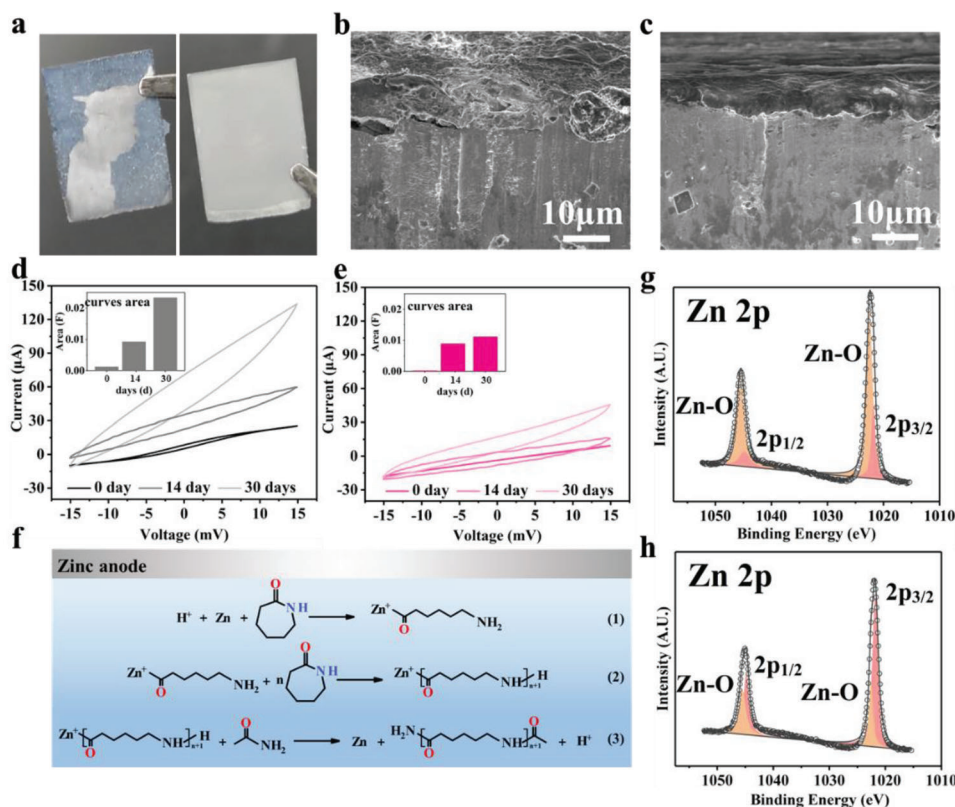
Figure 2. Surface state analysis of Zn foils in DES50 and DES0 electrolytes. a) Digital photograph of Zn foils soaking in DES0 (left) and DES50 (right) for 30 days at 60 °C temperature. Cross profiles SEM images of Zn foils soaking in b) DES0 and c) DES50 for 14 days at 25 °C; CV curves and their integral areas of Zn||Zn symmetric cells testing immediately, 14 days later, 30 days later with d) DES0 electrolyte and e) DES50 electrolyte. f) Mechanism diagram of the amides polymerizing to the membrane on the anode surface; XPS spectra of Zn 2p of Zn foils surface soaking in g) DES0 and h) DES50 electrolytes for 14 days.

a long chain. The degree of polymerization is significantly affected by the ratio of caprolactam to acetamide. If n is a positive number greater than 1, it can result in the growth of excessive chain segments, leading to increased surface polarization. Conversely, if n is less than 1, the polymerization process may terminate prematurely, resulting in incomplete surface protection.

$$ \tag{1} $$
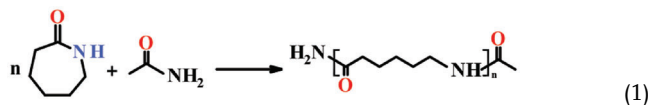
These observations align well with the electrochemical performance of the Zn||Zn symmetric cells, as depicted in Figure S15 (Supporting Information). The polarization increases with an increasing amount of caprolactam, which can be attributed to the thickening of the protective film. Furthermore, the formation of a protective membrane significantly enhances the cycle stability of Zn||Zn symmetric cells. To validate the effectiveness of this SEI membrane in ensuring battery stability, a series of experiments were conducted. Initially, the Zn foil was immersed in the DES50 electrolyte, and the pre-treated Zn foil was then assembled into symmetric cells. The resulting cells exhibited superior cycling performance compared to those assembled with the

DES0 electrolyte (Figure S16, Supporting Information). Moreover, when the Zn||Zn symmetric cells were cycled in the DES50 electrolyte for 10 cycles and subsequently reassembled with the DES0 electrolyte, the cells showed enhanced cycling stability, further demonstrating the effectiveness of the protective membrane (Figure S17, Supporting Information).

X-ray photoelectron spectroscopy (XPS) was performed to analyze the composition of the protective membrane on Zn foils immersed in DES0 and DES50 for 14 days. The Zn 2p peaks revealed a higher proportion of Zn-O species in the DES0 group compared to the DES50 group (Figure 2g,h), indicating a greater degree of surface oxidation in DES0 that could potentially compromise the stability of the Zn anode. In the O 1s spectra, an additional peak near 531.34 eV was observed (Figure S18, Supporting Information), and in the N 1s spectra, the peak corresponding to N–C = O around 400 eV was prominently seen in the DES50 group (Figure S19, Supporting Information). These peaks correspond to the characteristic functional groups of amides. This suggests that the DES undergoes polymerization, leading to the formation of a membrane that adheres to the surface of the Zn anode. Interestingly, the C 1s peaks of the DES50 group exhibited an increased intensity of the C = O peak at ≈288.34 eV, while the C–F peak originating from OTf⁻ at around 289.64 eV diminished (Figure S20, Supporting Information). These changes suggest effective inhibition of the corrosion caused by OTf⁻ in the DES50

**ADVANCED
SCIENCE NEWS**

www.advancedsciencenews.com

**ADVANCED
MATERIALS**

www.advmat.de
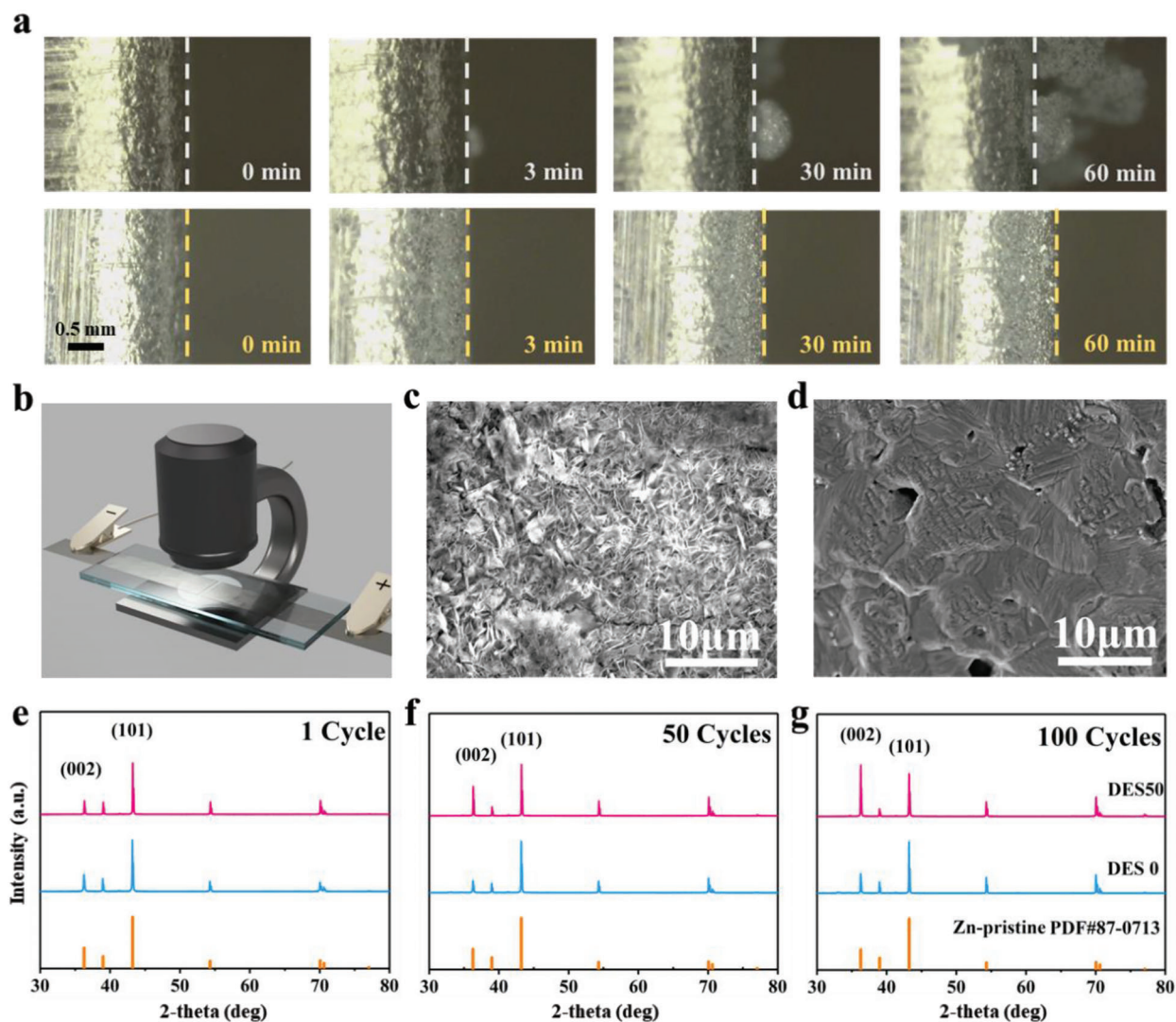
Figure 3. Zn plating/stripping and deposition behaviors. a) In situ optical microscopic observation of dendrite growth in DES0 and DES50 at a current of 20 mA cm^{-1}; b) schematic diagram of in situ microscopic observation equipment. Comparison of SEM images of Zn anode surface after 100 cycles in c) DES0 and d) DES50 at 1 mA cm^{-2} with a capacity of 1 mAh cm^{-2} and XRD patterns of Zn anode after e) 1 cycle; f) 50 cycles and g) 100 cycles.

group, highlighting its superior performance in mitigating OTf$^-$-related corrosion.[22]

In summary, DES50 outperformed DES0 as an electrolyte for Zn foils. It exhibited reduced capacitance, thinner corrosion layer, lower impedance, and slower rate of corrosion. The combination of caprolactam, acetamide, and Zn metal facilitates the formation of a protective film on the Zn anode surface, enhancing its stability and inhibiting further corrosion. The observed polarization trends, electrochemical performance, and cycle stability improvement demonstrate the efficacy of the protective membrane in maintaining battery stability.

2.3. Zn Deposition Behavior in DES-Based Electrolyte

In our study, we developed a unique in situ optical Zn||Zn symmetric cell (as depicted in **Figure 3**b) to observe the depositional

behavior of Zn^{2+}. The cell was constructed using two microslides sealed with UV-curing glue capable of withstanding the electrolyte. The surface of the cell was electronically isolated by a PVDF film, leaving only the cross-section part exposed for Zn deposition. Details of the cell fabrication can be found in SI. The applied current density during the experiment was 20 mA cm^{-2}. As shown in Figure 3a and Movie 2 (Supporting Information), during the deposition process, we observed that when the deposition reached 1 mAh cm^{-2} (3 min), the DES0 group started to exhibit uneven nucleation sites. As the deposition process continued, significant differences became apparent. The DES0 group exhibited the formation of Zn dendrites, indicative of non-uniform deposition. In contrast, the DES50 group displayed uniform nucleation-growth behavior. These results emphasize the significance of controlling the solvation structure of Zn ions to achieve uniform deposition and prevent the formation of undesirable structures.

2306546 (6 of 10)

ADVANCED
SCIENCE NEWS
www.advancedsciencenews.com

**ADVANCED
MATERIALS**
www.advmat.de

To further investigate the microstructural differences in Zn deposition with different electrolytes, we conducted a comparative test using Zn||Zn symmetric cells under a current density of 1 mA cm^{-2} and a capacity of 1 mAh cm^{-2}. After 100 cycles, we examined the morphology of the Zn foil, revealing significant differences between the two electrolytes. In the DES0 electrolyte, Zn deposition exhibited a flake-like structure with a high surface area, accompanied by the formation of cracks under the low current density conditions (Figure 3c). In contrast, the surface of the Zn foil in the DES50 electrolyte appeared flat and smooth, with a significantly reduced surface area (Figure 3d).

To gain deeper insights into these observed differences, we conducted X-ray diffraction (XRD) analysis of the anode samples after 1 cycle, 50 cycles, and 100 cycles. The XRD analysis provided valuable information about the crystallographic structure of the deposited Zn. The XRD analysis revealed significant differences between the DES50 and DES0 electrolytes. In the DES50 group, the intensity ratio of the (002) to (100) crystal planes increased from 0.38 to 1.2 after 100 cycles, indicating a pronounced preference for Zn ion growth along the (002) plane (Figure 3e–g). This preference for (002) plane growth promotes a more uniform and homogeneous deposition of Zn. In contrast, the DES0 group maintained a constant intensity ratio dominated by the (002) crystal plane throughout the cycling process, indicating a lack of preference for crystal plane growth and resulting in random deposition of Zn. These findings emphasize the crucial role of the electrolyte composition in influencing the crystallographic structure of the deposited Zn.

Additionally, the improved deposition behavior observed in the DES50 electrolyte is further supported by the nucleation process and cycling reversibility. We conducted tests on the nucleation overpotential of Zn ions under a current density of 5 mA cm^{-2}, and the results demonstrated a decrease from 474.3 to 228.1 mV, indicating a reduced kinetic hindrance for nucleation. Similar results were obtained under a current density of 10 mA cm^{-2} (Figure S21, Supporting Information). The unique solvation structure of Zn ions can facilitate the dynamic processes and lay the foundation for uniform Zn deposition.

2.4. Electrochemical Performance of DES-Based Electrolyte

The Coulombic efficiency (CEs) of the DES50 and DES0 electrolytes were evaluated using a modified Aurbach's method in Zn||Ti cells (**Figure 4**a).[23] To eliminate the substrate's influence, excess Zn was pre-deposited onto Ti foils prior to cycling. The CE of the DES50 electrolyte was found to be 98.37%, significantly higher than the 78.18% observed with the DES0 electrolyte. This substantial difference in CEs demonstrates that DES50 greatly enhances the reversibility of Zn-ions, further highlighting its superior performance. The photographs of a Zn||Zn symmetric cell, taken during Zn deposition and dissolution inside a glass bottle, clearly illustrate the differences between the two electrolytes (Figure 4b). The applied current density was 1 mA cm^{-2}, and the capacity was set at 1 mAh cm^{-2}. In the DES0 electrolyte, noticeable growth of Zn dendrites can be observed, and a significant amount of detached Zn particles can be seen after cycling for 30 cycles. On the other hand, the symmetric cell using the DES50 electrolyte demonstrates a uniform and dense deposition of Zn

throughout the cycling process. After 50 cycles, the Zn foil was removed from the cell and rinsed with deionized water. It was evident that the foil maintained its integrity and uniformity in the DES50 electrolyte, while in the DES0 electrolyte, the dissolution of Zn appeared to resemble pitting corrosion, resulting in the formation of numerous holes and pits on the surface of the foil.

The cycling performances of Zn||Zn symmetric cells were evaluated under various current densities. In Figure 4c, the Zn plating/stripping behavior at a current density of 1 mA cm^{-2} and a capacity of 1 mAh cm^{-2} is shown for both DES50 and DES0 electrolytes. It is evident that both electrolytes exhibit similar polarization voltages of ≈50 mV, indicating comparable rates of mass transport. However, the presence of the unique solvation structure and effective protection offered by DES50 significantly enhance the performance of the Zn anode, leading to a remarkable lifespan of over 2000 h. In contrast, the cycling life of Zn||Zn symmetric cells using DES0 electrolyte is less than 200 h. Moreover, impressive stability was achieved at higher current densities and capacities. As depicted in Figure 4d, a stable cycling duration of 1000 h was achieved at a current density of 10 mA cm^{-2} and a capacity of 10 mAh cm^{-2}. Furthermore, Figure 4e demonstrates a cycling duration of 250 h at a current density of 10 mA cm^{-2} and a capacity of 20 mAh cm^{-2}. Figure 4f displays the photographs of Zn||Zn pouch cells after 400 h of cycling at a current density of 1 mA cm^{-2} and a capacity of 1 mAh cm^{-2}. The pouch cell with DES0 electrolyte exhibits significant bloating and gas generation, whereas the DES50 group maintains its integrity without any signs of gas evolution. These observations confirm that the gas generation, primarily caused by HER, is effectively suppressed in the DES50 electrolyte, which is aligned with our previous findings. These results demonstrate the excellent performance of the DES50 electrolyte, showcasing its strong potential for practical applications.

The electrochemical stability window of an electrolyte is crucial for its application in batteries and full cells. In our previous investigation of the HER reaction, DES50 demonstrated a lower reduction onset potential compared to DES0, with a reduction potential shifted by 0.2 V. Additionally, the LSV curves depicted in Figure S22 (Supporting Information) revealed that DES50 exhibited a higher oxidation potential of 2.4 V versus Zn, while DES0 displayed an oxidation potential of around 2.2 V. The distinctive solvation structures of DES50 and DES0 contribute to the broadening of both the oxidation and reduction potentials.

To further investigate the practical application potential of the DES50 electrolyte, we constructed full cells with a VS$_2$ cathode in a VS$_2$||Zn configuration. The cyclic voltammetry (CV) curves of the VS$_2$||Zn cells in DES0 and DES50 electrolytes are depicted in **Figure 5**a. The CV curves exhibit two characteristic reduction/oxidation peaks corresponding to the V^{2+} to V^{3+} and V^{3+} to V^{4+} transitions in VS$_2$.[24] In DES0 electrolyte, the oxidation peaks occur at ≈0.7 and 0.8 V, while the reduction peaks are observed around 0.7 and 0.6 V. On the other hand, in DES50 electrolyte, a slight increase in polarization of ≈50 mV is observed, which can be attributed to the lower ionic conductivity of the DES50 electrolyte. However, despite this polarization, the accumulated CV curve area of DES50 is 17% higher than that of DES0, indicating enhanced reaction kinetics and higher capacity.

**ADVANCED
SCIENCE NEWS**

www.advancedsciencenews.com

**ADVANCED
MATERIALS**

www.advmat.de
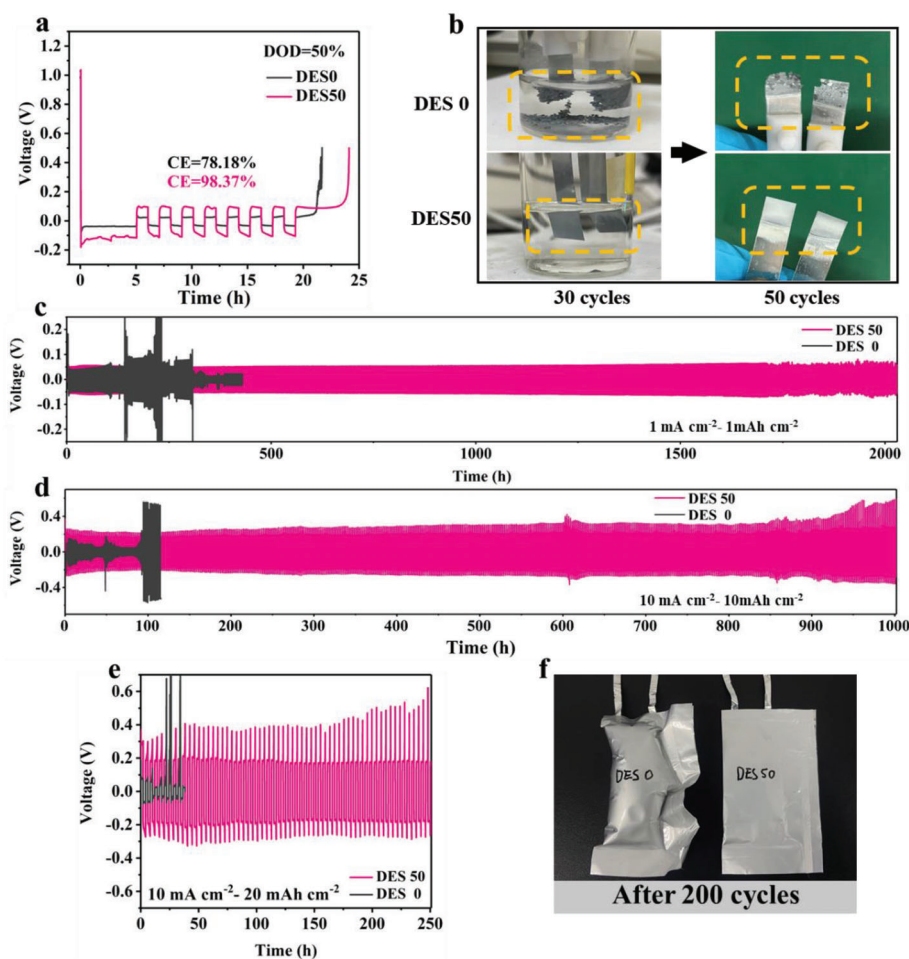
Figure 4. a) The comparison of Coulombic efficiency in DES0 and DES50 electrolytes at 50% DOD; b) Digital photograph of Zn foils cycling in DES0 and DES50 electrolyte for 30 cycles and 50 cycles at a current of 1 mA cm^{-2} and a capacity of 1 mAh cm^{-2}; Long-term galvanostatic cycling of Zn∥Zn symmetric cell with DES50 and DES0 electrolytes at c) 1 mA cm^{-2} −1 mAh cm^{-2}; d) 10 mA cm^{-2} −10 mAh cm^{-2} and e) 10 mA cm^{-2} −20 mAh cm^{-2}; f) Macroscopic flatulence of pouch cells in DES0 and DES50 electrolyte.

The rate performance of the VS$_2$∥Zn cell is presented in Figure 5b, accompanied by the charge and discharge curves illustrated in Figure S23 (Supporting Information). It can be observed that DES50 exhibits superior rate performance up to a current density of 0.5 A g^{-1}, while DES0 demonstrates higher capacity at higher current densities, specifically 1 A g^{-1}, which may be attributed to the occurrence of larger polymerization processes under these conditions. However, DES50 displays enhanced cycling stability compared to DES0. Figure 5c shows that at a current density of 0.1 A g^{-1}, the initial specific capacity of VS$_2$ is 185 mAh g^{-1}, and after 150 cycles, DES50 retains a specific capacity of 160.8 mAh g^{-1} with a capacity retention of 89.9%. In contrast, DES0 electrolyte only maintains a capacity of 95.32 mAh g^{-1} under the same conditions. The charge and discharge voltage profiles depicted in Figure S24 (Supporting Information) reveal that the charge and discharge potentials exhibit stable polarization over 150 cycles in the DES50 electrolyte. In contrast, in the DES0 electrolyte, the polarization continues to increase. This voltage fading cannot be solely attributed to the corrosion and accumulation of by-products on the Zn surface but also to the degradation of the cathode's intercala-

tion structure. After cycling, the concentration of vanadium ions in the DES50 electrolyte is significantly lower than that in the DES0 electrolyte. These findings suggest that DES50 can effectively inhibit ionic dissolution of the positive electrode (Figure S25, Supporting Information), thereby resulting in better cycling performance.

Long-term cycling tests were performed at a current density of 0.5 A g^{-1}. As depicted in Figure 5d, both electrolytes exhibit similar initial capacity at around 135 mAh g^{-1}. The DES50 electrolyte demonstrates an initial specific capacity of 133.81 mAh g^{-1} and maintains a capacity of 113.66 mAh g^{-1} after 500 cycles, with a capacity retention of 85.4%. In contrast, the DES0 group exhibits poor capacity retention, with only 47.2% (65.12 mAh g^{-1}) remaining after 500 cycles. These results further confirm the superiority of DES50 in terms of electrode stabilization and capacity preservation.

3. Conclusion

This study introduces a novel deep eutectic solvent (DES)-based electrolyte consisting of equal molar ratios of acetamide and

**ADVANCED
SCIENCE NEWS**

www.advancedsciencenews.com

**ADVANCED
MATERIALS**

www.advmat.de
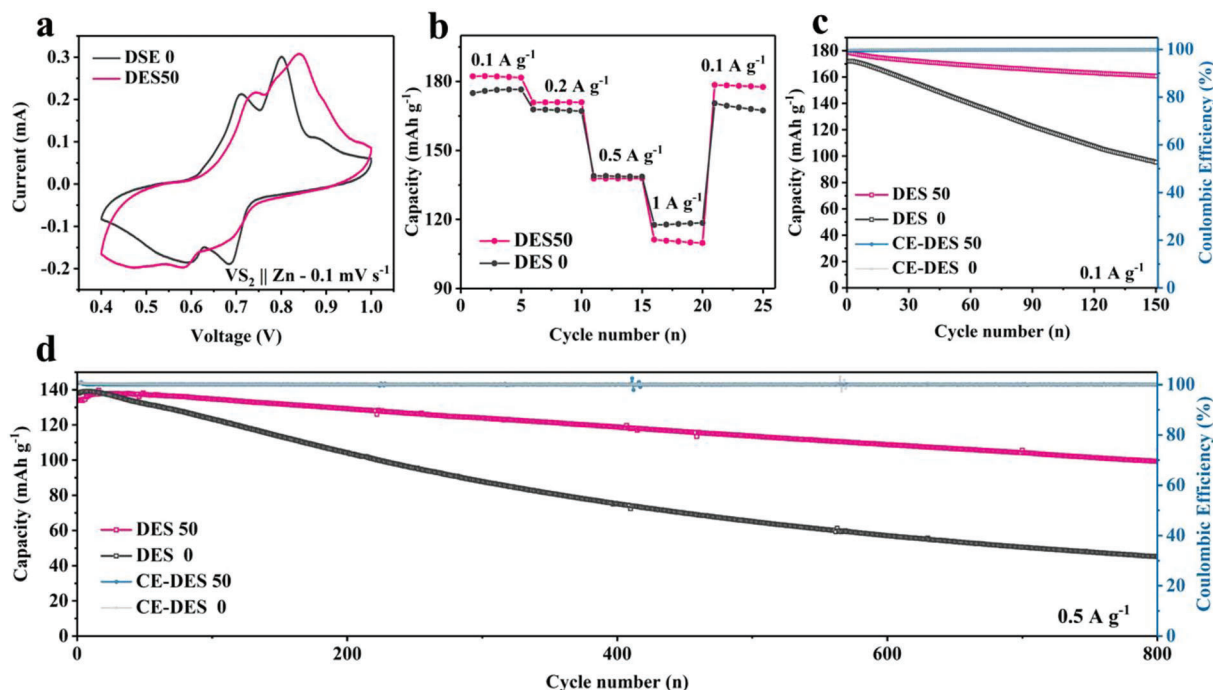
Figure 5. Electrochemical performance of VS_2||Zn cells operated in DES50 and DES0. a) CV curves of VS_2 cathode; b) Rate performance; c,d) Long-term cycling performance of VS_2||Zn full cell at 0.1 A g^{-1} and 0.5 A g^{-1}.

caprolactam with 50 vol% H_2O, along with 1 M $Zn(OTf)_2$ salt. Through a combination of theoretical analysis and experimental investigations, we have successfully demonstrated the remarkable capabilities of this electrolyte. Our findings reveal that the DES-based electrolyte efficiently reconstructs the solvation structure of Zn^{2+}, leading to the formation of a protective membrane on the Zn anode surface. This solvation structure effectively hinders the migration of solvated water molecules and mitigates the occurrence of the HER during the Zn deposition process. The in situ generated membrane acts as a protective barrier, further reducing the reactivity of water and minimizing the formation of undesirable by-products. Moreover, the DES50 electrolyte exhibits remarkable improvements in the suppression of Zn dendrite formation and facilitates more stable stripping/plating processes dominated by the Zn (002) crystal plane. Notably, our DES50 electrolyte demonstrates outstanding electrochemical performance, enabling stable stripping/plating for extended periods of up to 2000 h at 1 mAh cm^{-2} and 1000 h at 10 mAh cm^{-2} in Zn||Zn symmetric cells. Additionally, VS_2||Zn full cells utilizing DES50 electrolyte exhibit remarkable capacity retention of 85.4% after 500 cycles at 0.5 A g^{-1} and 89.9% after 150 cycles at 0.1 A g^{-1}.

This study represents a significant advancement in the design of multifunctional DES-based electrolytes for high-performance energy storage devices. The utilization of DES50 electrolyte demonstrates remarkable improvements in various key aspects, including stability, suppression of zinc dendrite formation, reduction of unwanted side reactions, and enhanced capacity retention. These findings hold great promise for the practical application of AZIBs and pave the way for future advancements in the field.

4. Experimental Section

Electrolyte Preparation: Acetamide (C_2H_5NO, Adamas, 98%+) and caprolactam ($C_6H_{11}NO$, Adamas, 98%+) were combined in a 1:1 molar ratio and heated in a 60°C oven for 1 h to obtain a clear and transparent liquid, referred to as the deep eutectic solvent (DES). Zinc trifluoromethane sulfonate ($Zn(CF_3SO_3)_2$, Adamas, 99%+) was then dissolved in the DES to create a DES with 1 M $Zn(OTf)_2$ as the solute. The resulting DES mixture was further diluted with deionized water using varying volume ratios of H_2O (65, 60, 55, 50, 45, and 40 vol%) to obtain the final electrolytes (DES35, DES40, DES45, DES50, DES55, and DES60). Additionally, a control group electrolyte (DES0) was prepared by dissolving zinc trifluoromethane sulfonate with a concentration of 1 M in deionized water.

Electrode Preparation: The purchased Zn foil (thickness: 50 μm, purity: 99.999%, Wenghou Metal Materials Co., Ltd.) was polished with a polishing cloth and washed with ethanol to remove the passivation layer. Then, the Zn foil was cut into discs ($\varphi = 12$ mm) to be used as a Zn electrode. The Ti foil (thickness: 20 μm, purity: 99.999%, Wenghou Metal Materials Co., Ltd.) was also scrubbed with mirror paper soaked with ethanol and cut into discs ($\varphi = 12$ mm) to be used as a Ti electrode. The cathode was prepared by mixing the VS_2 powder, super-P carbon and polyvinylidene fluoride (PVDF) in N-methyl-2-pyrrolidone (NMP) with a mass ratio of 7:2:1. Then, casting the slurry on the stainless-steel mesh and drying at 60 °C oven overnight. At last, the cathode was obtained by cutting the mesh with 2.8–3.1 mg cm^{-2} VS_2 into discs ($\varphi = 12$ mm).

Characterization: X-ray diffraction (XRD) patterns were obtained using a Bruker D8-Advance powder X-ray diffractometer operating at 40 kV and 30 mA, with Cu Kα radiation ($\lambda = 0.15\,405$ nm). X-ray photoelectron spectroscopy (XPS) measurements were performed on the American Thermo Fisher Scientific ESCALAB 250Xi, with a sputtering rate of 0.46 nm S^{-1}. The morphologies and structure of the Zn anode were examined using field emission Scanning Electron Microscopy (SEM, FEI, QUANTA 250FEG) at an accelerated voltage of 10 kV. Fourier transform infrared (FTIR) spectra were recorded using a Bruker VERTEX 70 FTIR spectrometer. For the in

situ observation of Zn^{2+} deposition, an optical microscope (AM4113T5, Dino Lite) was employed.

Electrochemical Measurements: All the CR2032-type cells were assembled in the open-air atmosphere using glass fiber filter (GF/D, Whatman) as the separator, and the electrolyte amount used in them was all 120 µL. They were all carried out by Neware test system (CT-4008, Neware) at 25 °C. Then, cyclic voltammetry (CV), linear sweep voltammetry (LSV), Tafel curves and electrochemical impedance spectroscopy (EIS) curves were all carried out on an electrochemical workstation (GAMRY INTERFACE 1010E). The frequency range of the EIS curves was set from 0.1–100 000 Hz and a voltage amplitude of 10 mV.

Molecular Dynamics (MD) Simulations: Gromacs program was used to simulate all-atom optimized potentials for liquid simulations (OPLS-AA) force field with resp charge.[25] The visualization of the simulations was performed using vmd. The initial model of the system was constructed using packmoL.[26] The total computation time was 25 ns, with each step consisting of a 2 fs time increment. The data from the last 5 ns of the simulation were used for analysis. The NPT ensemble was employed, with Nose-Hoover temperature control set at 25 °C and Berendsen pressure control at one atmosphere. The LINCS method was used to constrain all bond lengths involving hydrogen atoms. Electrostatic interactions were evaluated using the Particle Mesh Ewald (PME) method, and van der Waals interactions were calculated using a cutoff of 1 nm.

Supporting Information

Supporting Information is available from the Wiley Online Library or from the author.

Acknowledgements

Conflict of Interest

The authors declare no conflict of interest.

Data Availability Statement

The data that support the findings of this study are available from the corresponding author upon reasonable request.

Keywords

[1] a) B. Obama, *Science* **2017**, *355*, 126; b) D. Chao, W. Zhou, F. Xie, C. Ye, H. Li, M. Jaroniec, S.-Z. Qiao, *Sci. Adv.* **2020**, *6*, 4098.

[2] Z. Cai, Y. Ou, J. Wang, R. Xiao, L. Fu, Z. Yuan, R. Zhan, Y. Sun, *Energy Storage Mater.* **2020**, *27*, 205.

[3] a) S. Clark, A. R. Mainar, E. Iruin, L. C. Colmenares, J. A. Blázquez, J. R. Tolchard, A. Latz, B. Horstmann, *J. Mater. Chem.* **2019**, *7*, 11387; b) P. Wang, S. Liang, C. Chen, X. Xie, J. Chen, Z. Liu, Y. Tang, B. Lu, J. Zhou, *Adv. Mater.* **2022**, *34*, 2202733.

[4] a) P. Ruan, X. Chen, L. Qin, Y. Tang, B. Lu, Z. Zeng, S. Liang, J. Zhou, *Adv. Mater.* **2023**, *35*, 2300577; b) H. Zhang, Y. Zhong, J. Li, Y. Liao, J. Zeng, Y. Shen, L. Yuan, Z. Li, Y. Huang, *Adv. Energy Mater.* **2023**, *13*, 2203254.

[5] N. D. Ingale, J. W. Gallaway, M. Nyce, A. Couzis, S. Banerjee, *J. Power Sources* **2015**, *276*, 7.

[6] a) Q. Zhang, J. Luan, L. Fu, S. Wu, Y. Tang, X. Ji, H. Wang, *Angew. Chem., Int. Ed.* **2019**, *58*, 15841; b) B. Li, K. Yang, J. Ma, P. Shi, L. Chen, C. Chen, X. Hong, X. Cheng, M.-C. Tang, Y.-B. He, F. Kang, *Angew. Chem., Int. Ed.* **2022**, *61*, e202212587; c) Y. Song, P. Ruan, C. Mao, Y. Chang, L. Wang, L. Dai, P. Zhou, B. Lu, J. Zhou, Z. He, *Nano-Micro Lett.* **2022**, *14*, 218; d) H. Yan, C. Han, S. Li, J. Liu, J. Ren, S. Yang, B. Li, *Chem. Eng. J.* **2022**, *442*, 136081.

[7] X. Zeng, J. Mao, J. Hao, J. Liu, S. Liu, Z. Wang, Y. Wang, S. Zhang, T. Zheng, J. Liu, P. Rao, Z. Guo, *Adv. Mater.* **2021**, *33*, 2007416.

[8] W. Xu, K. Zhao, W. Huo, Y. Wang, G. Yao, X. Gu, H. Cheng, L. Mai, C. Hu, X. Wang, *Nano Energy* **2019**, *62*, 275.

[9] a) R. Zhao, H. Wang, H. Du, Y. Yang, Z. Gao, L. Qie, Y. Huang, *Nat. Commun.* **2022**, *13*, 3252; b) F. Wan, L. Zhang, X. i. Dai, X. Wang, Z. Niu, J. Chen, *Nat. Commun.* **2018**, *9*, 1656; c) H. Wang, H. Du, R. Zhao, Z. Zhu, L. Qie, J. Fu, Y. Huang, *Adv. Funct. Mater.* **2023**, *33*, 2213803.

[10] L. Geng, J. Meng, X. Wang, C. Han, K. Han, Z. Xiao, M. Huang, P. Xu, L. Zhang, L. Zhou, L. Mai, *Angew. Chem., Int. Ed.* **2022**, *61*, e202206717.

[11] Z. Li, Y. Liao, Y. Wang, J. Cong, H. Ji, Z. Huang, Y. Huang, *Energy Storage Mater.* **2023**, *56*, 174.

[12] L. Suo, O. Borodin, T. Gao, M. Olguin, J. Ho, X. Fan, C. Luo, C. Wang, K. Xu, *Science* **2015**, *350*, 938.

[13] A. S. Etman, M. Carboni, J. Sun, R. Younesi, *Energy Technol.* **2020**, *8*, 2000358.

[14] a) Z. Zhao, J. Lai, D. T. Ho, Y. Lei, J. Yin, L. Chen, U. Schwingenschlögl, H. N. Alshareef, *ACS Energy Lett.* **2023**, *8*, 608; b) H. Qiu, X. Du, J. Zhao, Y. Wang, J. Ju, Z. Chen, Z. Hu, D. Yan, X. Zhou, G. Cui, *Nat. Commun.* **2019**, *10*, 5374.

[15] Y. Yang, S. Liang, B. Lu, J. Zhou, *Energy. Environ. Sci.* **2022**, *15*, 1192.

[16] W. Kao-Ian, R. Pornprasertsuk, P. Thamyongkit, T. Maiyalagan, S. Kheawhom, *J. Electrochem. Soc.* **2019**, *166*, A1063.

[17] M. Han, J. Huang, X. Xie, T. C. Li, J. Huang, S. Liang, J. Zhou, H. J. Fan, *Adv. Funct. Mater.* **2022**, *32*, 2110957.

[18] X. Lin, G. Zhou, M. J. Robson, J. Yu, S. C. T. Kwok, F. Ciucci, *Adv. Funct. Mater.* **2022**, *32*, 2109322.

[19] J. Shi, T. Sun, J. Bao, S. Zheng, H. Du, L. Li, X. Yuan, T. Ma, Z. Tao, *Adv. Funct. Mater.* **2021**, *31*, 2102035.

[20] C. Zhang, L. Zhang, G. Yu, *Acc. Chem. Res.* **2020**, *53*, 1648.

[21] Z.-Y. Wu, W. Xu, Y.-C. Liu, J.-K. Xia, Q.-X. Wu, W.-J. Xu, *J. Appl. Polym. Sci.* **2009**, *113*, 2109.

[22] L. Zhang, L. Miao, W. Xin, H. Peng, Z. Yan, Z. Zhu, *Energy Storage Mater.* **2022**, *44*, 408.

[23] D. Aurbach, O. Youngman, Y. Gofer, A. Meitav, *Electrochim. Acta* **1990**, *35*, 625.

[24] P. He, M. Yan, G. Zhang, R. Sun, L. Chen, Q. An, L. Mai, *Adv. Energy Mater.* **2017**, *7*, 1601920.

[25] M. J. Abraham, T. Murtola, R. Schulz, S. Páll, J. C. Smith, B. Hess, E. Lindahl, *SoftwareX* **2015**, *1–2*, 19.

[26] L. Martínez, R. Andrade, E. G. Birgin, J. M. Martínez, *J. Comput. Chem.* **2009**, *30*, 2157.

ADVANCED MATERIALS

Supporting Information

Acetamide-Caprolactam Deep Eutectic Solvent-Based Electrolyte for Stable Zn-Metal Batteries

Shihe Wang, Ganxiong Liu, Wang Wan, Xueyang Li, Ju Li* and Chao Wang*

Supporting Information

Acetamide-caprolactam deep eutectic solvent-based electrolyte for stable Zn-metal batteries

Shihe Wang[†], Ganxiong Liu[†], Wang Wan, Xueyang Li, Ju Li*, Chao Wang**

Synthesis of VS₂ nanosheets: VS_2 powder was synthesized through a hydrothermal method.[27] Briefly, 0.234 g Ammonium Metavanadate (NH_4VO_3, Adamas, 99%) was dissolved in 30 mL deionized water and 2 mL $NH_3 \cdot H_2O$ and stirred for 1 h. Then, 1.13 g Thioacetamide (C_2H_5NS, Adamas, 99%) was added to the homogeneous mixture and continued to stir for 1 h. After that, the solution was transferred to a 50 mL Teflon-lined autoclave and heated at 180 °C for 20 h. Then, the samples were enduring a centrifugal washing by deionized water and ethanol 3 times, respectively. At last, the final product was dried at 60 °C for 8 h to obtain the black VS_2 powder. To verify the successful synthesis of VS_2, SEM, and XRD were used (Figure S26, S27).

Electrochemical measurements: CV curves were measured at a scan rate of 1 mV s^{-1}. The electrochemical windows of the electrolytes were measured using LSV curves scanning at 1 mV s^{-1} with Pt as the working and counter electrode, Ag/AgCl as the reference electrode. To prevent any interference from Zn deposition on the HER measurement, 1M NaOTf was chosen as the solute to exclude Zn from the system. The Tafel curves were tested using three electrode systems in an electrolytic tank, with Zn foil as the working electrode, Pt metal as the counter electrode, and Ag/AgCl as the reference electrode.

Differential scanning calorimetry analysis: Differential scanning calorimeter (DSC) was used to evaluate the phase-transition temperature of the mixtures with different acetamide/caprolactam molar ratios. Samples were scanned from -20 °C - 100 °C a rate of 5 °C min^{-1} under a nitrogen atmosphere.

Characterization: Inductively coupled plasma (ICP) was conducted on an Optical Emission Spectrometer (Optima 7300 DV). The batteries cycled in different electrolytes were disassembled and the obtained separators were immersed in 3 mL deionized water, then the supernatant was taken to measure the concentration of vanadium dissolving. The viscosity of

the electrolytes was measured on a digital viscometer (MSK-SFM-VT) at 25 °C. And the ions conductivity was measured on the conductivity meter (METTLER TOLEDO FE38) at 25 °C.

In-situ optical observation: The optical Zn‖Zn symmetric cell was conducted using a self-designed construction consisting of two grooved microslides. The use of thin and flat glass slides facilitated precise light focusing and enhanced observation. The grooves on the slides provided ample space for the electrolyte. Two Zn foils were placed between the microslides and securely sealed using a UV curing glue, ensuring a tight enclosure. A total of 100 μL of electrolyte was used in the setup. Both sides of the Zn foil were coated with a PVDF film, which was conducted using a doctor blade coating method with a slurry containing 3% PVDF in NMP. This process resulted in a PVDF coating layer with a thickness of approximately 15 μm. As a result, the deposition of Zn occurred specifically at the lateral edge, which had a deposition area of 0.005 cm^2. During the experiment, a constant current of 0.1 mA was applied, and the deposition process was continuously recorded using an optical microscope. This allowed for real-time observation and analysis of the Zn deposition behavior.

Capacitance calculation: During the non-faradaic intervals, the area enclosed by the cyclic voltammetry (CV) curve can provide insights into the interface capacitance behavior to some extent. The specific equivalent capacitance can be calculated using equation (1).[28]

$$C = \frac{1}{Ev} \int_{V1}^{V2} i\, dV \qquad (1)$$

In this case, E represents the potential window, which is calculated as the difference between the upper bound (V_2) and the lower bound (V_1) of the potential range. The scan rate is denoted by v, the discharge or charge current is represented by i, and dV represents infinitesimal changes in potential.

The electric double-layer capacitance (C_{dl}) was calculated by analyzing the non-Faraday interval of the double-layer capacitor current in CV curves at different scan rates. A linear fitting method was employed to determine the C_{dl} value.

$$i_c = dq/dt = d(C_{dl}\varphi)/dt = C_{dl}(d\varphi/dt) + \varphi(dC_{dl}/dt) \qquad (2)$$

$$dC_{dl}/dt = 0,\ d\varphi/dt = v \qquad (3)$$

The double-layer current (i_c) is related to C_{dl} and the scan rate (v) by the equation $i_c = C_{dl}*v$. To determine the capacitance, the slope of the linear fitting of ic versus v is calculated. In this study, $i_c = (i_{0v+} - i_{0v-})/2$, where i_{0v+} and i_{0v-} represent the average values of the positive scan and negative scan at 0 V, respectively. This selection allows for a more accurate description of i_c.[29]
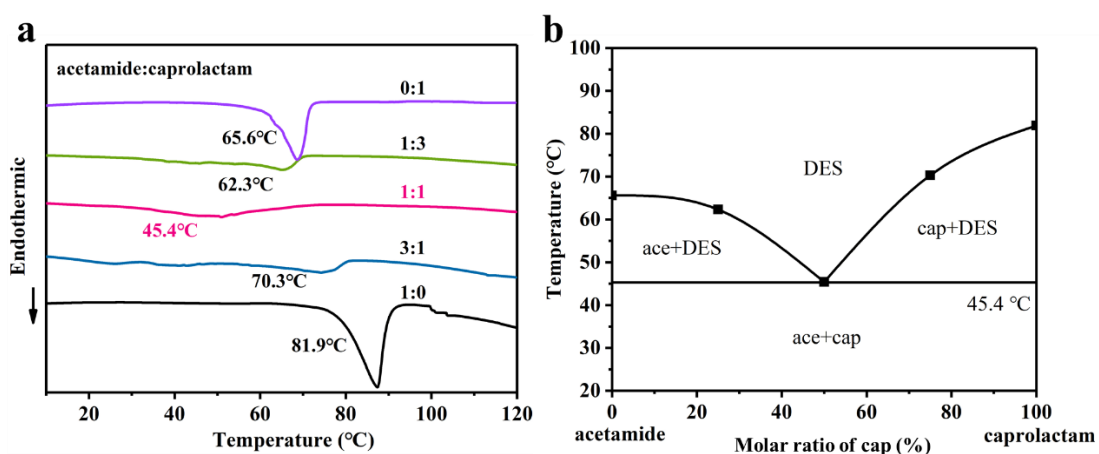
Figure S1. a) DSC curves and b) phase diagram of the acetamide-caprolactam DES with different ratios.
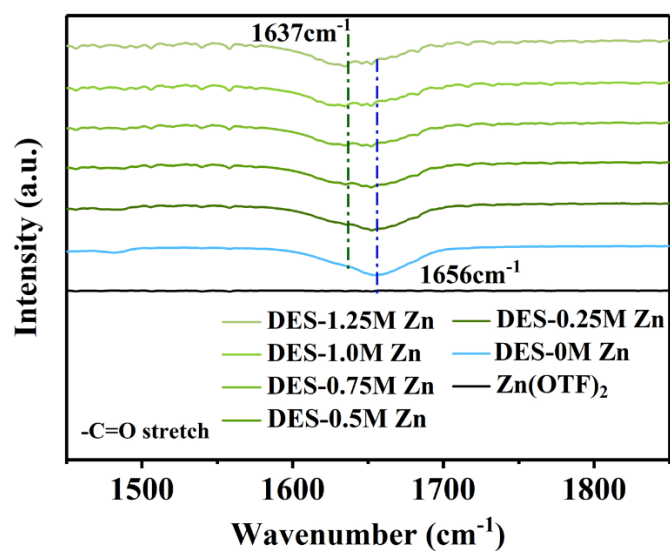
Figure S2. FT-IR spectra of DES with gradient concentration Zn(OTf)₂.
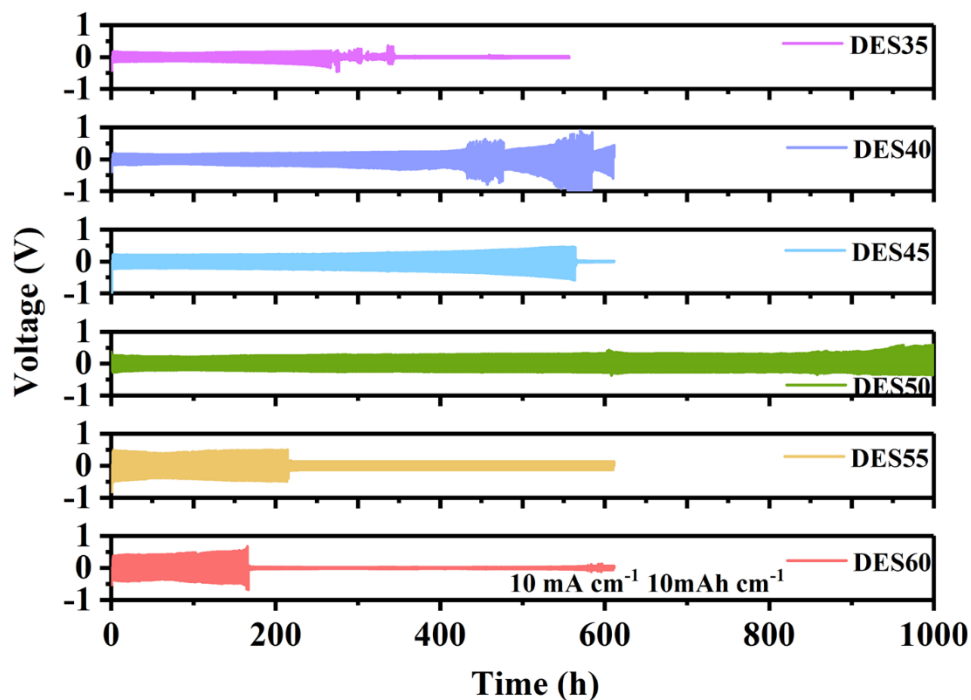
Figure S3. The voltage profiles of Zn‖Zn symmetric cells using DES containing gradient percent of H_2O as electrolyte at 10 mA cm^{-2} with a capacity of 10 mAh cm^{-2}.
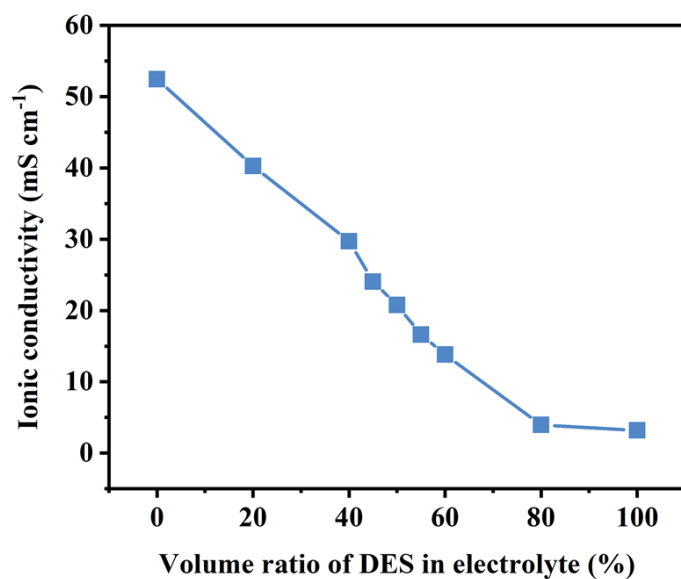
Figure S4. Ionic Conductivity of Electrolyte with different ratios of acetamide-caprolactam DES.
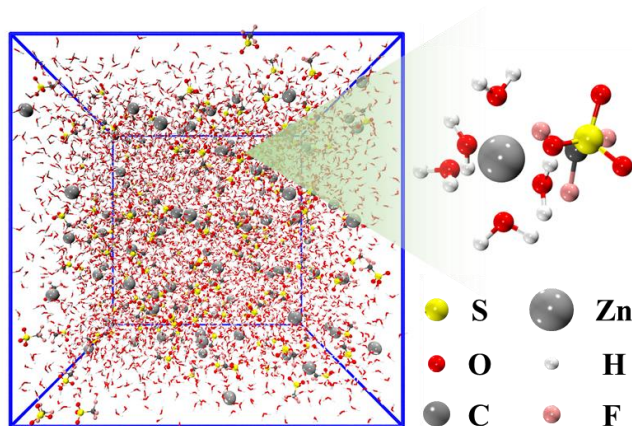
Figure S5. 3D snapshot obtained by MD simulations and representative Zn^{2+}-solvation structure of DES0.
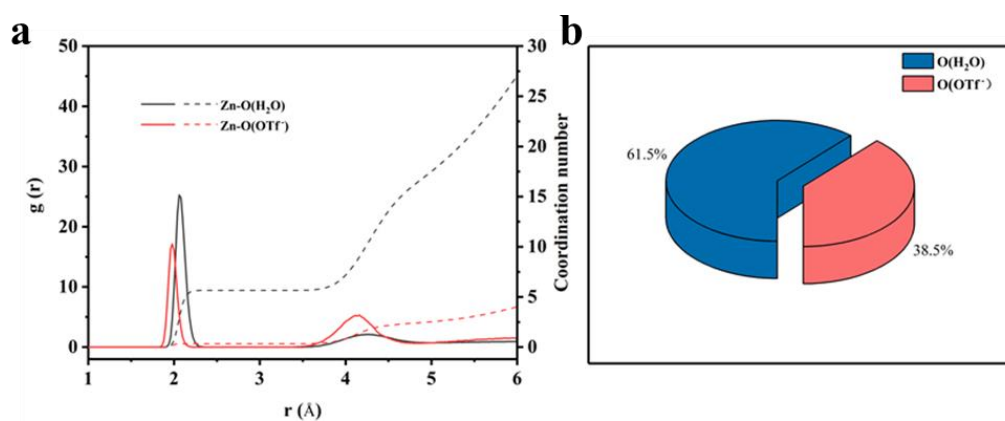
Figure S6. RDFs for Zn-O(H_2O), Zn-O(OTf$^-$) with coordination number of Zn^{2+} from MD simulations and distribution of coordination in primary solvation sheath in DES0.
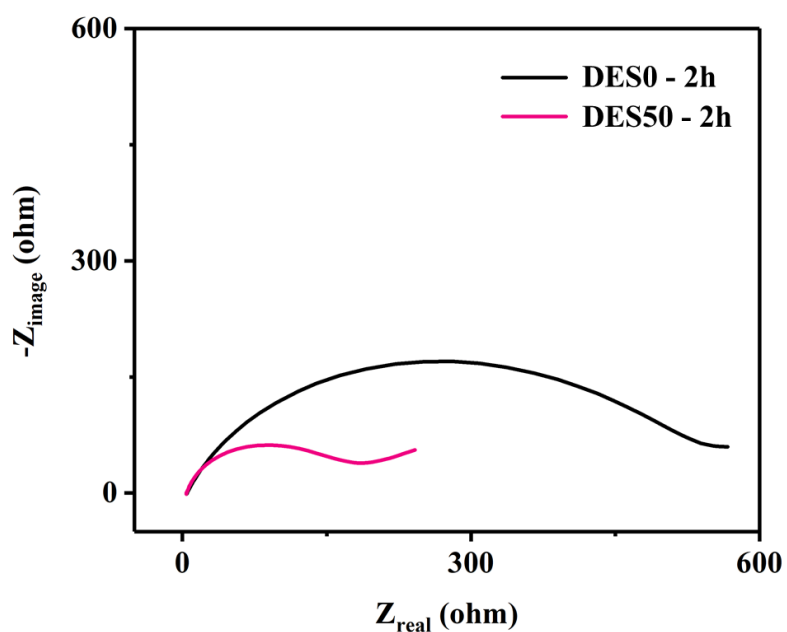
Figure S7. Electrochemical Impedance Spectroscopy (EIS) curves of Zn||Zn symmetric cells with a) DES0 and b) DES50.
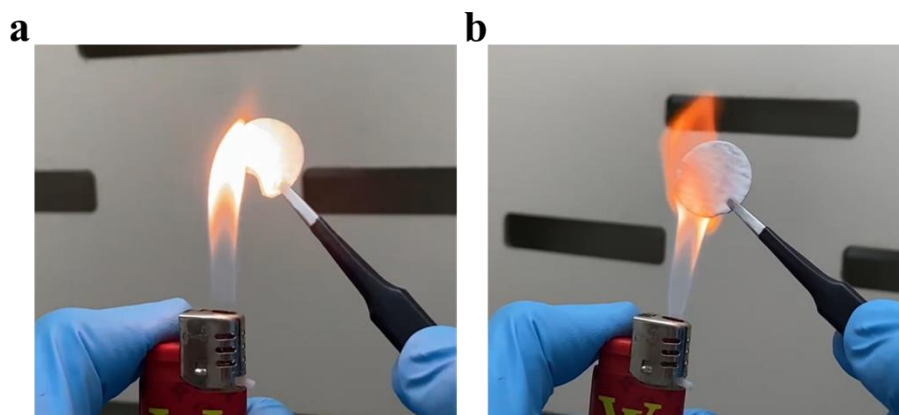
Figure S8. Flammability test of a) glass fiber separator and b) glass fiber separator stained with DES50.
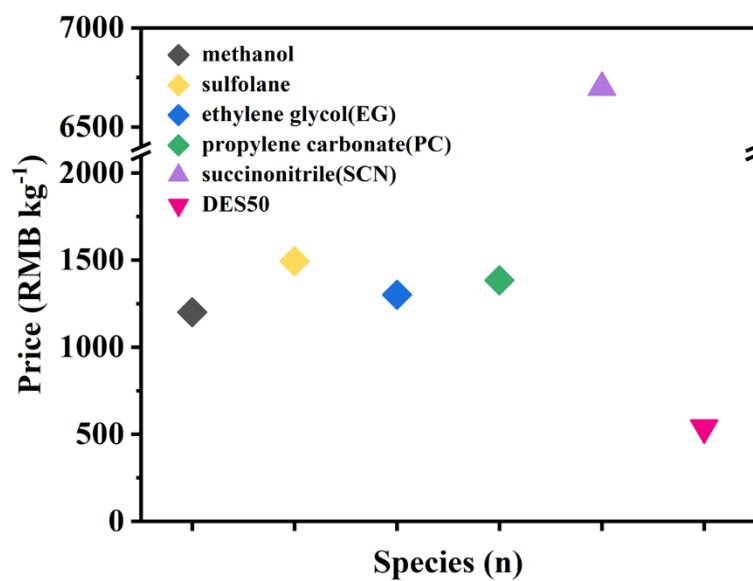
Figure S9. Price comparison of DES50's solvents with other common eutectic solvent species.
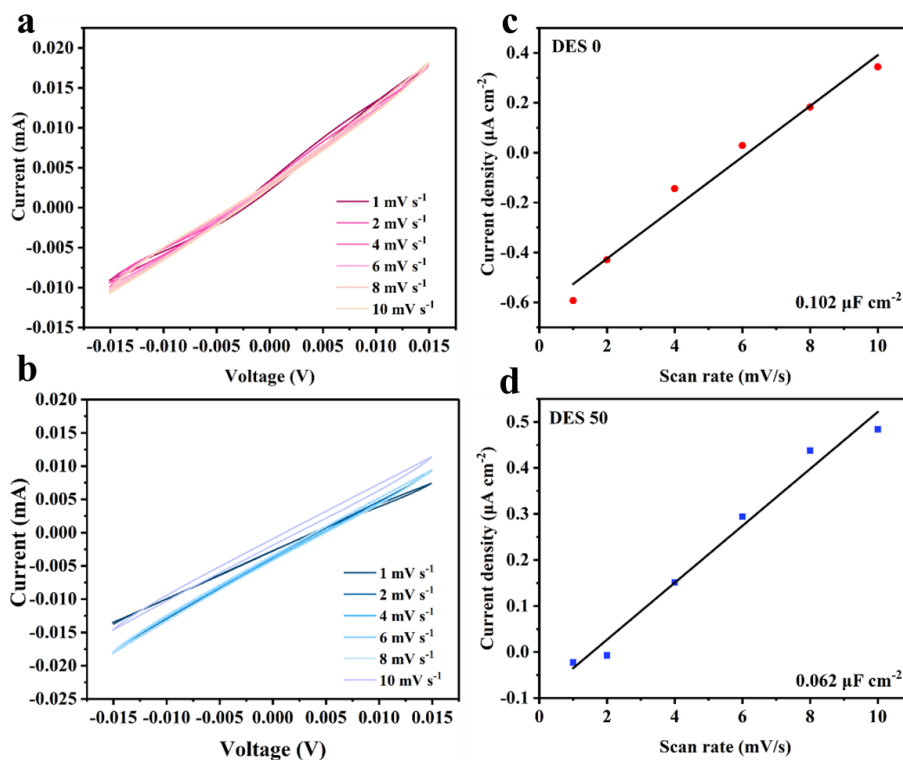
Figure S10. CV curves of Zn‖Zn symmetric cells in the voltage range of -15 mV to 15 mV using gradient scan rate in a) DES0 and b) DES50. Fitted curves of capacitive currents versus scan rate of the cells using c) DES0 and d) DES50.
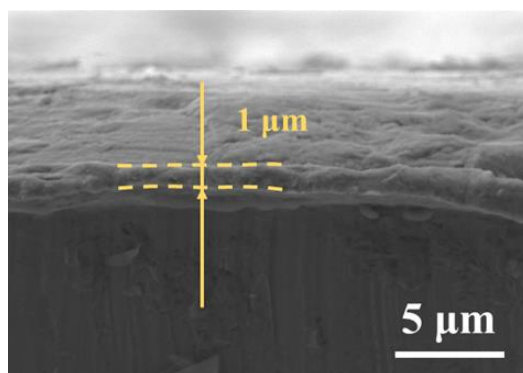
Figure S11. Cross profiles SEM images of Zn foils soaking in DES50 for 1 day at room temperature.
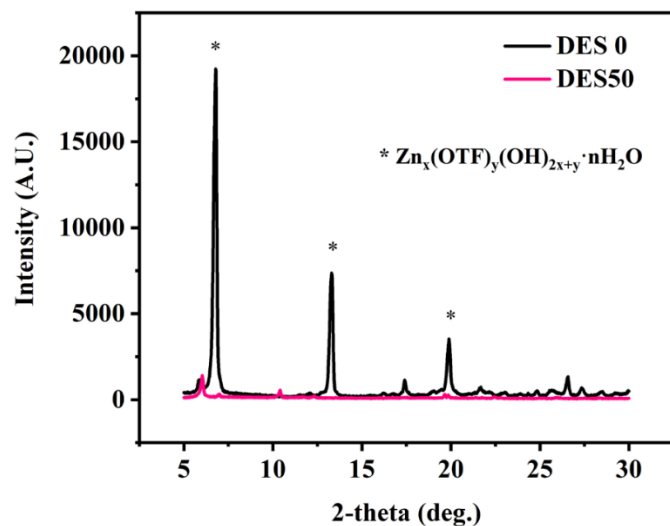
Figure S12. XRD patterns of Zn foils surface soaking in DES0 and DES50 for 14 days at room temperature.
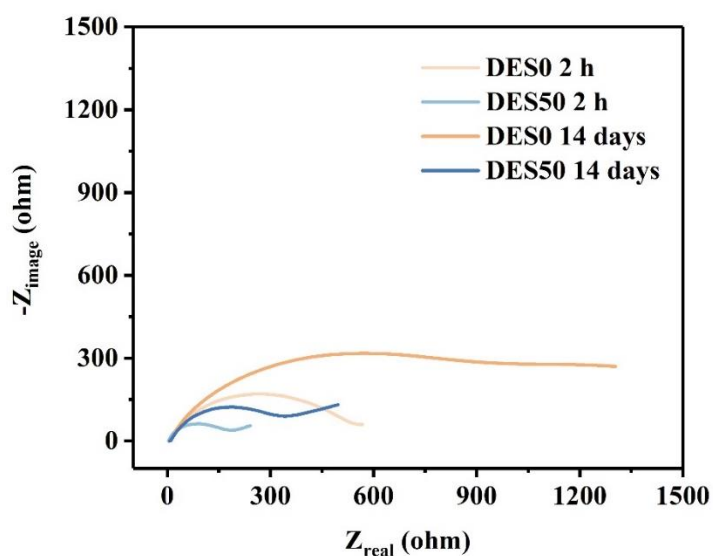
Figure S13. Electrochemical Impedance Spectroscopy (EIS) curves of Zn||Zn symmetric cells after different resting times.
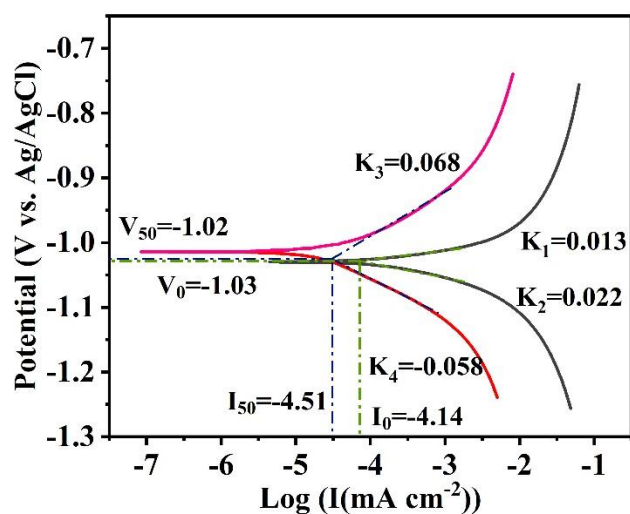
Figure S14. Tafel curve at a scan rate of 1 mV s^{-1} of Zn anodes in DES50 and DES0.
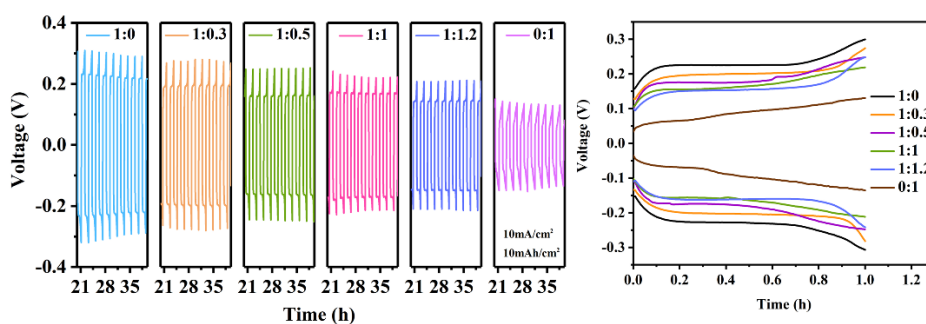
Figure S15. Comparison of polarization between different proportions of caprolactam and acetamide groups in Zn‖Zn symmetrical cells.
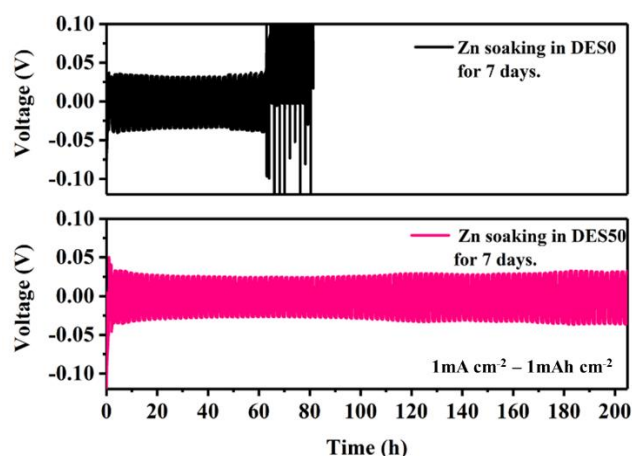
Figure S16. The voltage profiles of Zn‖Zn symmetric cells using the Zn electrodes soaking in DES0 and DES50 for 7 days and reassembling in DES0 electrolyte at the current of 1 mA cm^{-2} with the capacity of 1 mAh cm^{-2}.

9
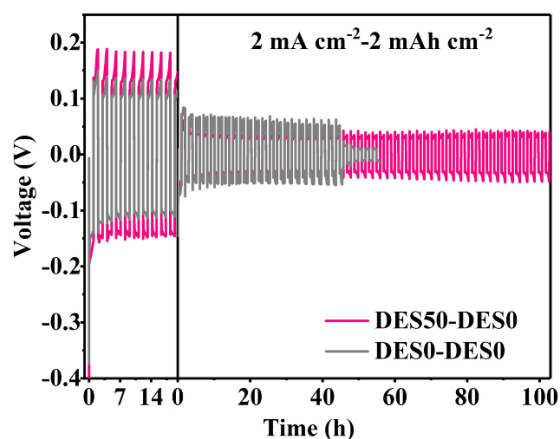
Figure S17. The voltage profiles of Zn∥Zn symmetric cells cycling at 2 mA cm^{-2} -2 mAh cm^{-2} conditions using diverse electrolyte in the first 10 cycles and the same DES0 electrolyte after 10 cycles. For better disassembly, two layers of separator were used in the first 10 cycles.
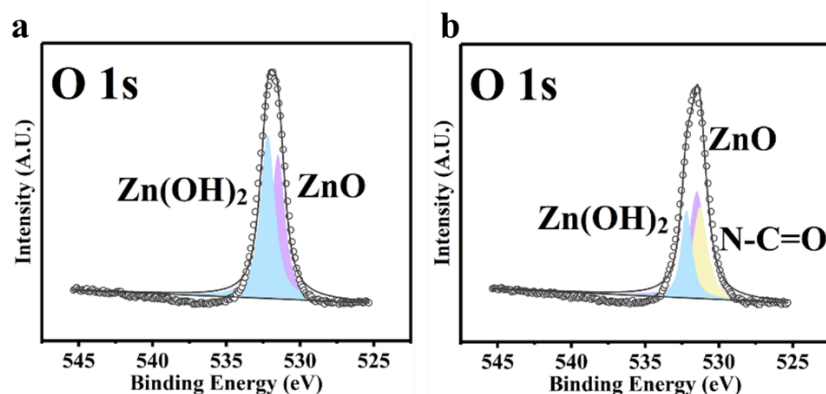
Figure S18. XPS spectra of O 1s of Zn foils surface soaking in a) DES0 and b) DES50 electrolytes for 14 days.
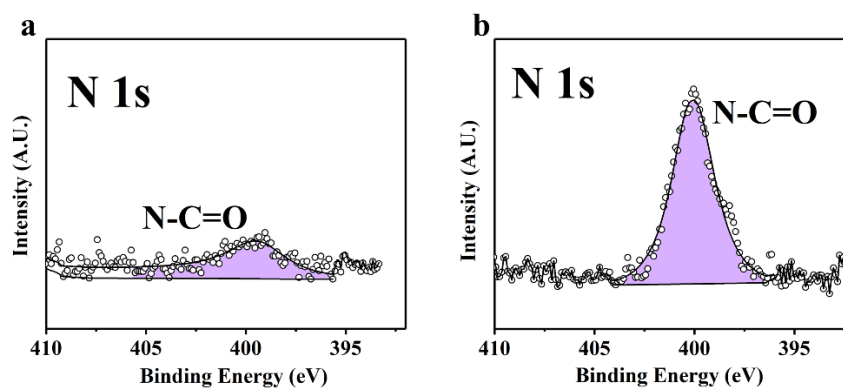
Figure S19. XPS spectra of N 1s of Zn foils surface soaking in a) DES0 and b) DES50 electrolytes for 14 days.
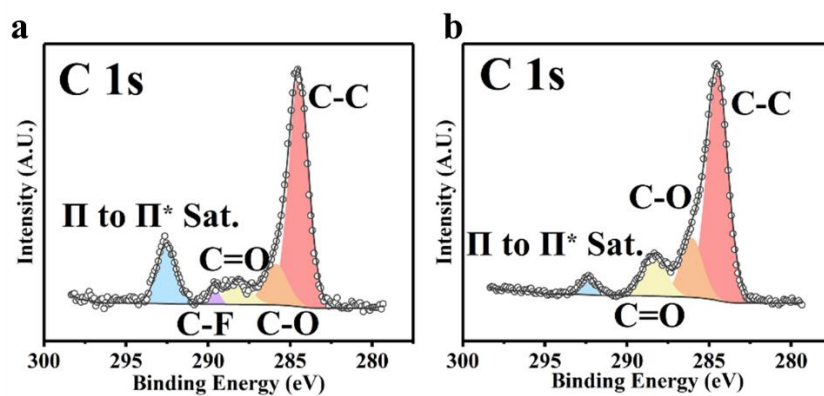
Figure S20. XPS spectra of C 1s of Zn foils surface soaking in a) DES0 and b) DES50 electrolytes for 14 days.
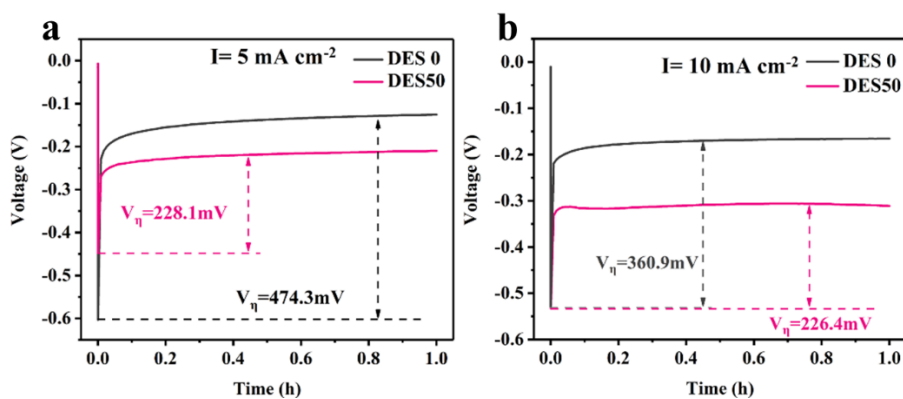
Figure S21. Nucleation overpotential of Zn anode in DES50 and DES0 at a current of a) 5 mA cm^{-2} and b) 10 mA cm^{-2}.

11
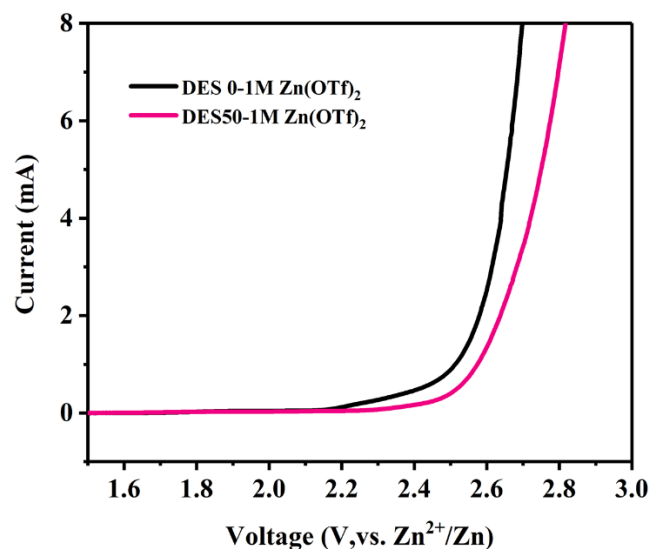
Figure S22. LSV curves of Zn electrode in DES0 and DES50 electrolytes at a scan rate of 1 mV s^{-1}.
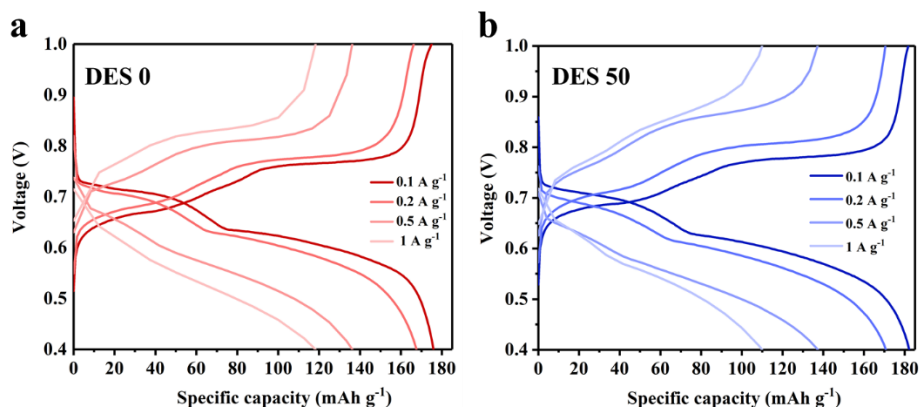
Figure S23. Galvanostatic charge/discharge profiles of VS$_2$‖Zn cells at various current densities in a) DES0 and b) DES50.
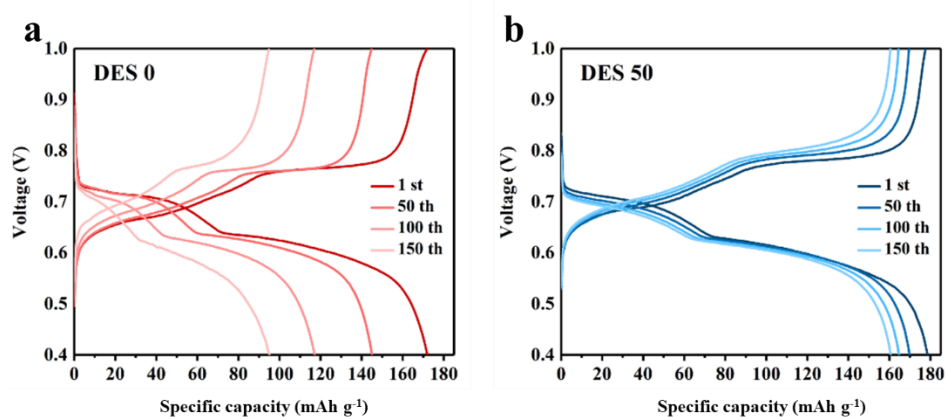
Figure S24. Galvanostatic charge/discharge profiles of VS$_2$‖Zn cells at various cycle numbers and the current of 0.1 A g^{-1} in a) DES0 and b) DES50.
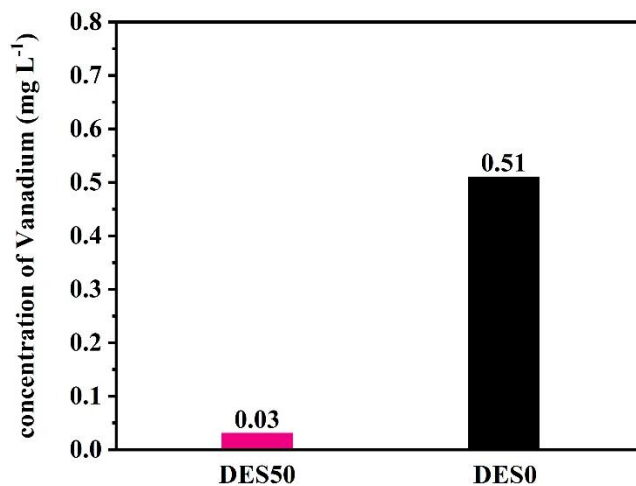
Figure S25. Concentration of vanadium dissolving in the electrolytes after 800 cycles.
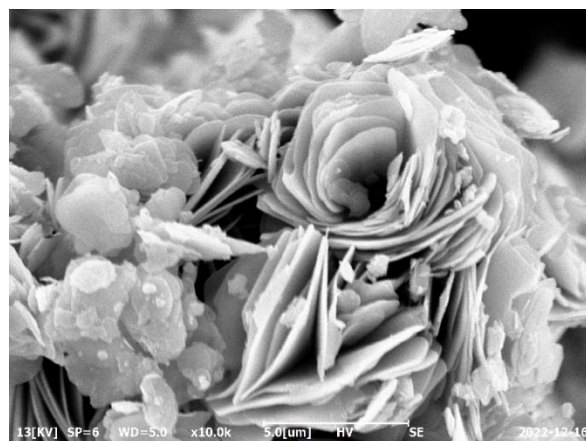
Figure S26. SEM image of VS$_2$ cathode materials.
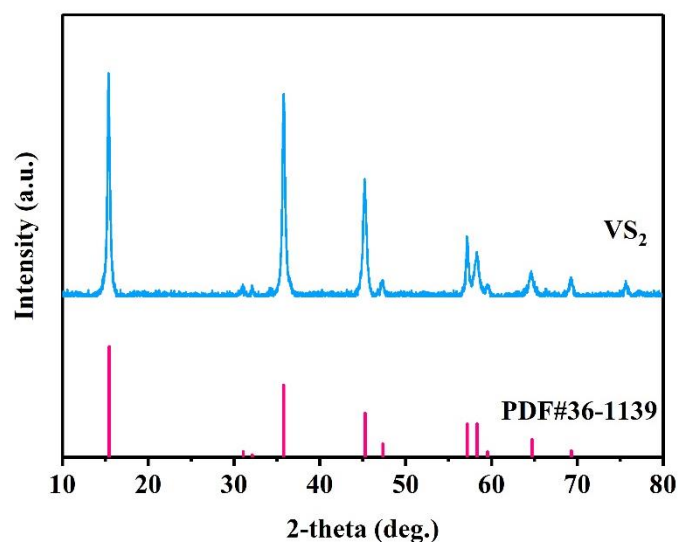
Figure S27. XRD pattern of VS$_2$ cathode materials.

Table 1. Summary of prices of various eutectic solvent species. Price data of all solvents were collected from Aldrich (https://www.sigmaaldrich.com/US/en).

species	Sigma Aldrich SKU	Online price (RMB)	Normalized price (RMB)
methanol	322415	950.39/L	1201.50/kg
sulfolane	T22209	746.34/500g	1492.68/kg
ethylene glycol(EG)	324558	1447.37/L	1300.42/kg
propylene carbonate(PC)	310328	1666.89/L	1383.66/kg

succinonitrile(SCN)	160962	3349.5/500g	6699/kg
caprolactam	C2204	447.07/kg	447.07/kg
acetamide	8.22343	857.27/kg	857.27/kg
DES50	\	\	536.05/kg

References

[1]   P. He, M. Yan, G. Zhang, R. Sun, L. Chen, Q. An, L. Mai, *Adv. Energy Mater.* **2017**, 7, 1601920.

[2]   T. S. Mathis, N. Kurra, X. Wang, D. Pinto, P. Simon, Y. Gogotsi, *Adv. Energy Mater.* **2019**, 9, 1902007.

[3]   L. M. Da Silva, L. A. De Faria, J. F. C. Boodts, *Electrochim. Acta* **2001**, 47, 395.